Journal of Hydrology 543 (2016) 782–795

Contents lists available at ScienceDirect

Journal of Hydrology

journal homepage: www.elsevier.com/locate/jhydrol

Research papers

Quantitative drought monitoring in a typical cold river basin over Tibetan Plateau: An integration of meteorological, agricultural and hydrological droughts

Godfrey Ouma Makokha [a,c,e], Lei Wang [a,b,c,*], Jing Zhou [a], Xiuping Li [a], Aihui Wang [d], Guangpeng Wang [a], David Kuria [e]

[a] Key Laboratory of Tibetan Environment Changes and Land Surface Processes, Institute of Tibetan Plateau Research, Chinese Academy of Sciences, Beijing, China
[b] CAS Center for Excellence in Tibetan Plateau Earth Sciences, Beijing, China
[c] University of Chinese Academy of Sciences, Beijing, China
[d] Nansen-Zhu International Research Center, Institute of Atmospheric Physics, Chinese Academy of Sciences, Beijing, China
[e] Dedan Kimathi University of Technology, Nyeri, Kenya

ARTICLE INFO

Article history:
Received 15 May 2016
Received in revised form 23 October 2016
Accepted 26 October 2016
Available online 1 November 2016

This manuscript was handled by Andras Bardossy, Editor-in-Chief

Keywords:
Standardized anomaly index
Cold river basin
Tibetan Plateau
Drought
WEB-DHM-S

ABSTRACT

We introduce a Rainfall, Snow and Glacier melt (RSG) standardized anomaly (SA) index to reflect water availability in cold river basins by taking into account snow and glacier melt that influence seasonal water availability. The study takes advantage of a high-resolution Water and Energy Budget-Based Hydrological Distributed Model with improved snow physics (WEB-DHM-S) at a grid size of 5 km to quantify hydrological regimes in a typical cold river basin in the Tibetan Plateau (Lhasa River basin as a demonstration site) from 1983 to 2012. Standardized anomaly index was utilized as drought Indicator whereby each meteo-hydrological parameter involved in drought quantification was fitted to a distribution pattern on a monthly basis. Akaike Information Criterion and Bayesian Information Criterion were used as selection criteria. Drought indices were computed from the model inputs and outputs, which included RSG for meteorological drought, soil moisture (surface and root-zone) for agricultural drought and discharge and groundwater level for hydrological drought. From spatial and temporal analyses, drought occurred in 1984, 1988, 1995, 1997, 2009 and 2010, with the highest severity in August, September, July, August, June and June, respectively. This study addresses the glacierized cold river basin's dryness by considering the contribution of snow and glacier in drought quantification, an integration of meteorological, agricultural and hydrological was performed to highlight drought hotspots in the Lhasa River Basin. To the best of our knowledge, this is the first drought study in Lhasa River Basin.

1. Introduction

Drought is one of the most expensive hydrological extremes, creeping phenomenon with undefined onset and end and therefore it is imperative to monitor and predict the likelihood of occurrence at the basin level (Nam et al., 2015; Zarafshani et al., 2016; Laaha et al., 2016; Ortega-Gaucin et al., 2016). Drought can occur in wet and humid regions despite its association to aridity, affecting agriculture, ecosystems and social sector (Carrão et al., 2016). The complexity of the cold region makes it even more complicated to estimate the magnitude of the drought due to the presence of glaciers and snow. The widely applied standardized precipitation index (SPI; McKee et al., 1993) has been used to characterize meteorological drought and by extension hydrological drought in areas where streamflow data are unavailable or were subjected to human intervention (Staudinger et al., 2014). However, SPI does not take into account temporary storage of solid precipitation and later melting of snow and glacier, thus resulting in significant differences between SPI and streamflow derived hydrological droughts as a result of time lag. As pointed out by the National Drought Mitigation Centre (see online at http://drought.unl.edu/DroughtBasics/TypesofDrought.aspx) meteorological drought can be defined as degree of dryness and duration of dryness. This dryness has solely been based on precipitation, but if you consider winter season in cold regions, precipitation mainly occurs in the solid state. The basin can receive an adequate amount of precipitation yet not all this water will be available in the liquid state (a lot

* Corresponding author at: Institute of Tibetan Plateau Research, Chinese Academy of Sciences, No. 16 Lincui Road, Chaoyang District, Beijing 100101, China.
E-mail address: wanglei@itpcas.ac.cn (L. Wang).

http://dx.doi.org/10.1016/j.jhydrol.2016.10.050
0022-1694/

of it will occur in the solid state (snowfall)) thus resulting in basin dryness. Likewise, during summer, basins in cold regions receive water from snowmelt and glacier melt adding to wet conditions from precipitation. RSG combines rain (the liquid part of precipitation), snowmelt and glacier melt forming liquid water that reaches basin surface to reflect the correct basin dryness or wetness hence the preference of RSG over precipitation to study meteorological droughts in the cold basin.

Drought severity is expressed in terms of a single number and is generally characterized by drought indices or statistics (Tsakiris et al., 2007; Heim, 2002). Table 1 shows meteorological conditions considered for a range of Standardized Anomaly index (SA) values. The conditions and range of SA conditions are same as those of SPI by McKee et al. (1993) as explained by Jaranilla-Sanchez et al. (2011). In general, there are four different types of drought: meteorological, agricultural, hydrological (physical characteristics; shown in Fig. 1) and socioeconomic (negative impacts on environmental and socioeconomic systems; Wilhite and Glantz, 1985; Tijdeman et al., 2015; Blauhut et al., 2015; Meresa et al., 2016). Meteorological drought depends only on precipitation deficit and duration of precipitation deficit. Agricultural drought refers to situations with insufficient soil moisture levels to meet the water needs of plants during the growing season (Hao and Singh, 2015; Shukla et al., 2011; Seçkin and Topçu, 2016). Hydrological drought occurs after a longer period of precipitation deficit (i.e., hydrological drought normally occurs after meteorological and agricultural drought) (Ceglar et al., 2008). Hydrological drought has been broadly studied within the last decades in many countries (Fleig et al., 2010; Hisdal and Tallaksen, 2003; Nalbantis and Tsakiris, 2009; Stefan et al., 2004; Tallaksen and Van Lanen, 2004), mainly due to increasing frequency of periods of drought in mild climate conditions where increasing air temperature, often combined with lack of precipitation causes a decrease in available water in river basins and in groundwater levels (Fendeková and Fendek, 2012; Esper et al., 2007). Processes and estimation methods for surface and groundwater droughts were analyzed in many drought studies (Meyboom, 1961; Mishra and Singh, 2010; Tallaksen and Van Lanen, 2004). Socioeconomic drought occurs when meteorological, agricultural or hydrological drought affects the supply of economic goods negatively and it usually occurs when the water supply is insufficient to meet human and environmental needs (Maia et al., 2015). Lhasa River basin has a harsh and unforgiving environment (remoteness, high altitude, inclement weather, etc.) with an average elevation of approximately 4500 m above mean sea level. The temperatures in the basin are cold, precipitation is sparse while oxygen and atmospheric pressure are low directly influence the human living conditions. Compared with low elevation areas, there are relatively few human activities in the basin because few people live in such harsh conditions. Due to the above factors, this study did not consider socio-economic drought as assessment of how drought affected people's behavior and options (e.g., water rationing, increased prices or lost recreational opportunities).

Table 1
Meteorological conditions considered for the range of SA values (Jaranilla-Sanchez et al., 2011).

SA values	Meteorological condition
2.0+	Extremely wet
1.5 to 1.99	Severely wet
1.0 to 1.49	Moderately wet
−0.99 to 0.99	Near normal
−1.49 to −1.0	Moderately dry
−1.99 to −1.5	Severely dry
−2 and less	Extremely dry

Recent advancement in drought quantification at the basin level has led to the use of a new standardized anomaly (SA) index based on hydrological model quantification of droughts and all types of droughts can be based on a single index (Jaranilla-Sanchez et al., 2011). We used the developed SA index to quantify the droughts of cold river basins where cryosphere components exist. However, the presence of snow and glaciers cannot be reasonably quantified by Jaranilla-Sanchez et al. (2011) approach, as there is temporary storage of water in solid form within cold river basins. During the cold period when temperatures are below freezing, precipitation occurs in a solid state and accumulation continues as long as temperatures are below freezing (Gao et al., 2012). The solid-state water is temporarily retained in the basin without accumulating in streams for domestic, agricultural and industrial use; thus, basing meteorological drought estimation on precipitation results into incorrect drought conditions as droughts can still occur despite available adequate precipitation during such a period. During warmer periods (temperatures above the freezing point), accumulated snow melt increases streamflow (Li et al., 2008). Besides snowmelt, glacier-melt also contributes significantly to overall discharge in a glaciated basin (Engelhardt et al., 2014). Snow and glacier melts are therefore key elements of discharge during late spring and summer in cold region basins as the magnitude and timing of runoff from such a catchment tend to be sensitive to changes in temperature due to its influence on snow and glacier melt (He et al., 2014). More recently, snow melt inclusion in drought index derivations has resulted into the Standardized Snow Melt and Rain Index (SMRI), developed by Staudinger et al. (2014) to improve drought estimation in cold regions. Staudinger et al. (2014) work need further improvement. First, the research focused on development of a rain and snowmelt index only, which alone cannot be relied upon as drought relates to multiple meteorological and hydrological variables (Hao and AghaKouchak, 2013; Hao et al., 2014) rather than comprehensively estimating the overall drought influence at the basin level by including other types of droughts. Secondly, the presence of glaciers in glacierized basin complicates the situation, as the developed measure does not consider glaciers. Finally, the method is a complementary index to SPI based on a Pearson type III distribution, which has been shown not to be good for variables other than precipitation (Shukla and Wood, 2008). This paper focuses on further improvement of this index, and the construction of a standardized anomaly index of rain, snowmelt and glacier melt to replace the original SPI (that could not represent available liquid water for current use in cold regions) for improved drought monitoring in cold regions as well as integrating different droughts in Lhasa River basin.

The objective of this study was to develop a new approach for quantitative drought monitoring in cold river basins, where total precipitation (liquid and solid forms) does not accurately represent water availability. The paper is organized as follows. Section 2 describes a distributed biosphere hydrological model and the SA index. The study area and datasets are introduced in Section 3. Section 4 depicts the evaluations of hydrological model, and quantitative drought monitoring at a typical cold region (Lhasa River Basin over Tibetan Plateau). Section 5 draws conclusions.

2. Method and model

2.1. Distributed biosphere hydrological model

The model is a coupled Water and Energy Budget-Based Distributed Hydrological Model (WEB-DHM; L. Wang et al., 2009a,b,c) with Simplified Simple Biosphere Scheme version 3 (SSiB3; Sun and Xue, 2001; Xue et al., 2003) three-layered energy balance snow scheme and Biosphere-Atmosphere Transfer (BATS; Dickinson

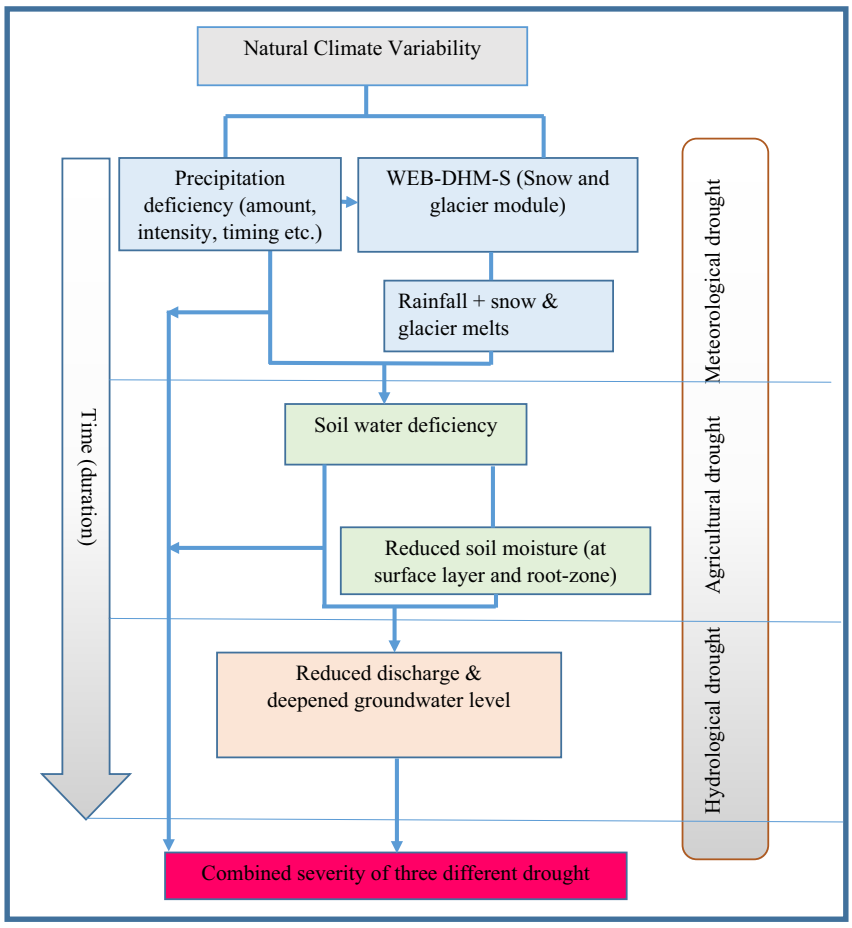

Fig. 1. The sequence of Drought impacts for meteorological, agricultural and hydrological drought.

et al., 1993; Yang et al., 1997) albedo scheme to improve snow physics and runs at an hourly time step at a predefined grid size (Shrestha et al., 2014b) (Fig. 2). Initially, WEB-DHM was developed by embedding a simple biosphere scheme (SiB2; Sellers et al., 1996) to a geomorphology-based hydrological model (GBHM; Yang et al., 2001; Wang and Wang, 2006). In various studies (Hu et al., 2015; Jaranilla-Sanchez et al., 2011; L. Wang et al., 2009c, 2010a,b, 2012; F. Wang et al., 2011, 2012; Xue et al., 2013; Zhou et al., 2015), WEB-DHM has been demonstrated as a distributed biosphere hydrological model that enables consistent descriptions of water, energy, and CO_2 fluxes at the basin scale.

The new coupling resulted in a more comprehensive simulation of snow variables such as density, water equivalent and the surface temperature of snow and snowmelt runoff, as well as liquid water and ice content in each snow layer (Shrestha et al., 2012). The point scale and basin scale evaluation of WEB-DHM-S (Shrestha et al., 2010) in wide regions showed that the model was able to simulate the variability of snow density, snow depth, snow water equivalent, snow albedo, snow layer temperature, snow cover area and runoff (Shrestha et al., 2014a). In WEB-DHM snow is considered as a constant density (200 kg m^{-3}), a single-layer bulk snow mass balance and thermal regime of snow is not distinguished from that of soil whereas, in WEB-DHM-S, Snow is divided into three layers. The top layer is kept at a constant 2 cm depth for diurnal changes in snow surface temperature. The middle layer is kept at a maximum thickness of 20 cm and the remaining body of snow is assigned to the bottom layer. The calculation of mass balance for each layer is dependent on precipitation, evaporation/condensation, compaction, liquid water retention, snow runoff and filtration into the underlying layers. The in-depth analysis of model equations and snow physics can be found in earlier studies (Shrestha et al., 2010, 2012). In this study, in addition to snow, the presence of glaciers in the basin was considered, with the glacier being simplified as thick snow (100 m) (Zhou et al., 2015). Pixels considered having glaciers were used to simulate glacier melt while in non-glacier pixels it was considered as snow. Although there are still uncertainties, glacial runoff simulation improves the accuracy of total runoff more than considering only rain and snow melt (Shrestha et al., 2015).

Various datasets were used in this study, including Digital Elevation Model (DEM), soil, land-use, Leaf Area Index (LAI), Fraction of Absorbed Photosynthetically Active radiation (FPAR), glacier and forcing data described in Table 2 were manipulated from the native resolution to a predefined 5-km size through inverse distance weighting (IDW) interpolation and nearest neighbor resampling before integration into WEB-DHM-S. Data collection in a mountainous region coupled with a climate of a cold region posed a large challenge in the acquisition of data. To overcome this challenge, some of the model input datasets (DEM, land-use, soil, glacier, LAI and FPAR) were subset from global datasets. The model was run at hourly time steps to output gridded RSG, groundwater level, soil moisture (surface and root-zone) and discharge, which this study utilized to effectively quantify droughts in this basin. The simulated discharge was compared to observed discharge in order to calibrate the model; the calibrated model results were compared with the observed data from different periods for validation. Simulated RSG was used to determine meteorological drought which was compared with precipitation (model input) and later

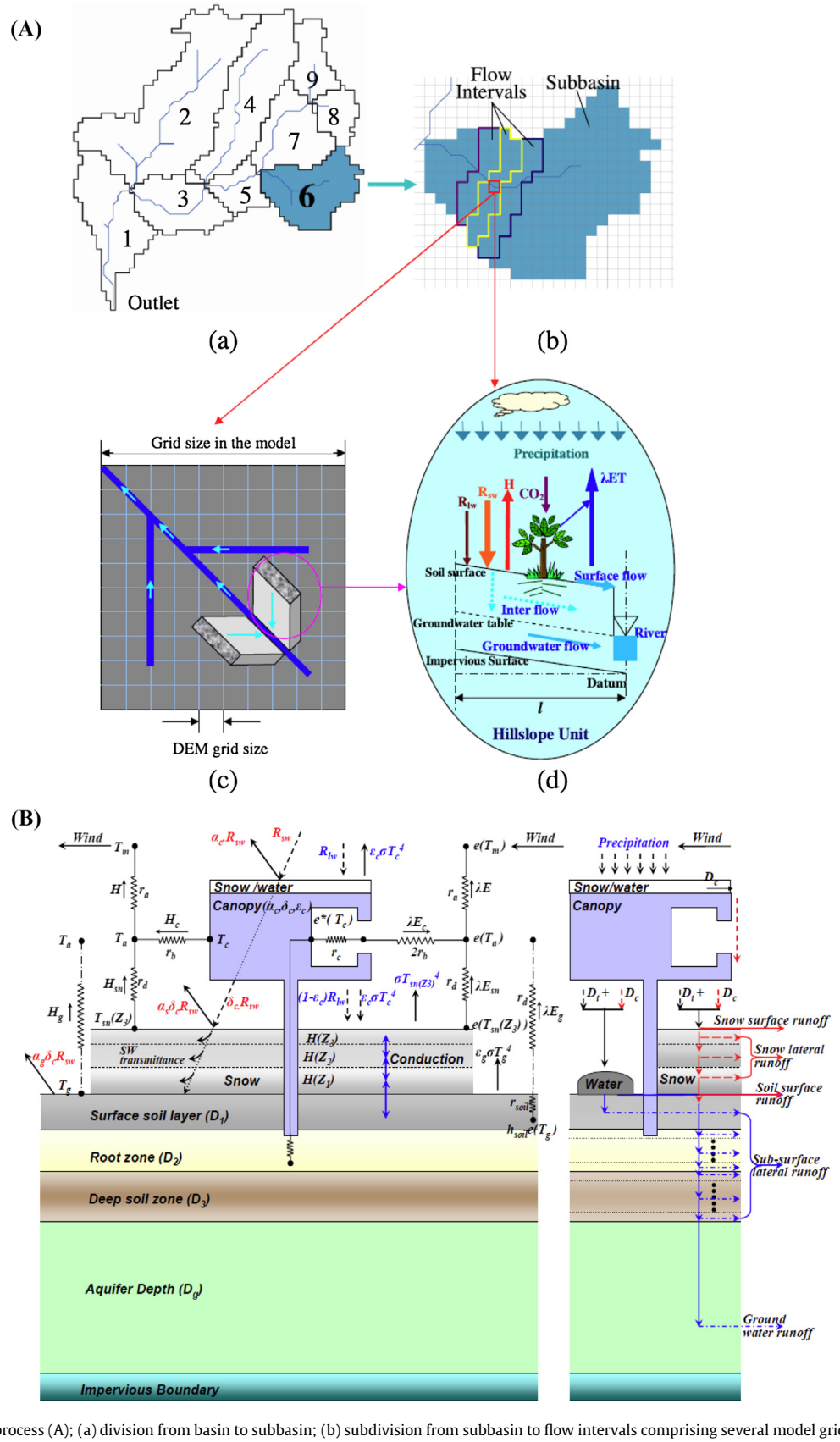

Fig. 2. The WEB-DHM process (A); (a) division from basin to subbasin; (b) subdivision from subbasin to flow intervals comprising several model grids; (c) discretization from a model grid to a number of geometrically symmetrical hillslopes; (d) and description of t the water moisture transfer from atmosphere to river. Rsw, Rlw, H are downward solar radiation, long wave radiation and sensible heat flux, respectively. (B) A detailed description of vertical 3-layer energy balance soil and Snow model coupled with WEB-DHM: Two different soil subdivision schemes are used for describing land-surface and hydrological processes, respectively. For snow model details are given by Shrestha et al. (2014a,b).

Table 2
Data sets utilized in WEB-DHM-S to simulate hydrological and meteorological variables and their sources.

Data	Description	URL
DEM	SRTM 90m	http://srtm.csi.cgiar.org/
Soil	FAO soil map with a spatial resolution of 5 arc minutes	http://www.fao.org/soils-portal/soil-survey/soil-maps-and-databases/harmonized-world-soil-database-v12/en/
Land use	USGS global land-use 1 km	http://edc2.usgs.gov/glcc/glcc.php
LAI/FPAR	AVHRR (1981–2001) 1 km	ftp://primavera.bu.edu/pub/datasets
	MODIS (2000 ~ now) 1 km	https://wist.echo.nasa.gov/~wist/api/imswelcome/
Glacier	WESTDC2.0 1 km	http://westdc.westgis.ac.cn
Forcing data	ITP forcing data 0.1 degrees	http://westdc.westgis.ac.cn

RSG and precipitation were related to observed discharge to determine the suitable parameter that can reveal cold basin dryness. Other simulated model outputs utilized in the study for various droughts were soil moisture (surface and root zone) for agricultural drought and discharge and groundwater level for hydrological drought.

The initial conditions of three hourly precipitation, air temperature, pressure, short and long wave radiation and specific humidity drove the point scale model simulation at the basin pour point at Lhasa hydrological station. In addition, the MODIS snow cover product, which has been widely used for snowmelt models (Klein and Barnett, 2003; Parajka and Blöschl, 2008; Tekeli et al., 2005), was utilized as well as glacier areal coverage to quantify liquid water. The model was calibrated based on daily-observed discharge. The two-step calibration was done from 2001 to 2005. In the first step, a long-term spin up period from 1983 to 2000 was selected in which model was run to generate initial conditions that were used in model calibration. Therefore, the first step provided a framework for the second step, which was purely based on trial and error method to optimize parameters by comparing simulated and observed streamflow. The calibration was done by adjusting saturated hydraulic conductivity for surface soil, anisotropy ratio which relates hydraulic conductivity in vertical and horizontal planes and maximum surface water storage (Jaranilla-Sanchez et al., 2010). This process accounts for all water from the surface flow, subsurface flow and base flow leading to streamflow. With good calibration results, the model simulated results can be relied upon.

The performance of the model was evaluated by comparing the simulated and observed discharges. The Nash-Sutcliffe (NS) model efficiency coefficient (Nash and Sutcliffe, 1970), Relative Error (RE), Root Mean Square Error (RMSE) and Mean Bias Error (MBE) were used as an evaluation criterion for simulated results. NS is defined as:

$$NS = 1 - \frac{\sum_{i=1}^{n}(Q_{oi} - Q_{si})^2}{\sum_{i=1}^{n}(Q_{oi} - \bar{Q}_{oi})^2} \quad (1)$$

where Q_{si} and Q_{oi} are simulated and observed discharge values respectively, $\bar{Q}_{oi}$ is mean discharge over entire study period while n is the total number of time series.

2.2. Standardized Anomaly index (SA)

The seasonal variation in basin parameters requires a method that will provide more information about the magnitude of the anomalies by removing the influence of dispersion. SA was preferred over the standardized index (SI) developed by McKee et al. (1993) due to limitations of SI discussed by Jaranilla-Sanchez et al. (2011). First, SI only utilizes a single gamma distribution, which tends to overlook differences in distribution patterns of data variation in mean monthly values. This might apply to some parameters like precipitation. However, it cannot be extended to all parameters and hence can only apply to specific parameters that follow a gamma distribution. Shukla and Wood (2008) evaluated the assertion by McKee et al. (1993) that a gamma distribution used for fitting precipitation can be extended to other variables by using it for the runoff. They found that distributions other than the gamma distribution would be more appropriate for the model-based runoff. In our study, several hydrological variables had varying monthly distributions. Individual variables were considered on a monthly basis to effectively fit the variables to an appropriate distribution (see Table 3). Statistical model selection is a trade-off between bias and variance. Akaike Information Criterion (AIC) and Bayesian Information Criterion (BIC) were preferred as selection criteria due to their ability to simultaneously compare multiple models, evaluate uncertainties in model selection and their simplicity in calculation from maximum likelihood estimates (Posada and Buckley, 2004). For this study, the best-fit model was selected on the basis of minimum corrected AIC (AIC_c) and BIC (BIC_c) (Jaranilla-Sanchez et al., 2011) which are defined as follows:

$$\mathrm{AICc} = -2\log\ \mathrm{likelihood} + 2\mathrm{k} + \frac{2k(k+1)}{n-k-1} \quad (2)$$

where k is the number of estimated parameters and n is the number of observations in the dataset.

$$\mathrm{BICc} = -2\log\ \mathrm{likelihood} + \mathrm{k}\ln(\mathrm{n}) \quad (3)$$

where n is the sample size.

The insensitivity of the SI with regard to seasonality and the monthly difference is a result of the utilization of a simple average of precipitation for each period. In dry climates, zero values will be common, as in the case of the Lhasa River Basin during the month of December, January and February, when there is very little or no precipitation. In such a case, a highly skewed underlying precipitation distribution and the limitation of the gamma distribution will result in a non-normal distribution for a short scale of time, causing errors in quantification of drought. Contrary to SI, the SA has the ability to show consequences of shortage or surplus in rainfall, which has better coherence with the consequences of drought and wet spells (Chanda and Maity, 2015).

SA can be defined as the conversion of variables (hydrological in this case) at a station into units of the monthly-based number of standard deviations from the long-term station mean. In order to calculate SA, the variables were fitted to a distribution pattern by considering AIC_c and BIC_c, transformed to a normal distribution as follows:

$$x_{transformed} = \frac{x-u}{\sigma} \quad (4)$$

where $u = \int xf(x)dx$, $\sigma = \sqrt{var(x)}$, $var(x) = \int (x-u)^2 (f(x)dx$ and $f(x)$ is the distribution function of any hydrological parameter x. Then standardized as follows,

$$\mathrm{SA} = \frac{\mathrm{x_{transformed}} - \bar{\mathrm{x}}_{\mathrm{transformed}}}{\sigma_{\mathrm{transformed}}} \quad (5)$$

where $\bar{x}_{transformed}$ is the long-term mean of transformed values while $\sigma_{transformed}$ is the standard deviation of the transformed parameter. This method adequately represents long-term variation in parameters, hence being ideal for drought analysis compared to other methods (Vicente-Serrano and López-Moreno, 2005). It can also be used across the board to analyze any kind of drought and thus

Table 3
Monthly best-fit distribution patterns for the different hydrological parameters.

Month	Precipitation	Discharge	Soil moisture: surface	Soil moisture: root zone	Groundwater level	Rain + snow/glacier melts
Jan	Log Generalized Gamma	Log Generalized Gamma	Normal	SEV	Normal	Log Generalized Gamma
Feb	Zero Inflated Lognormal	LEV	Normal	Weibull	Normal	Log Generalised Gamma
Mar	Log-logistic	Lognormal	Normal	Weibull	LEV	Log-logistic
Apr	Weibull	LEV	Weibull	Lognormal	Normal	Log-logistic
May	Log Generalized Gamma	Normal	Weibull	Normal	Normal	Weibull
Jun	Weibull	Normal	Logistic	Lognormal	Normal	Normal
Jul	Normal	Log Generalized Gamma	Normal	LEV	Normal	Normal
Aug	Lognormal	Normal	Weibull	LEV	LEV	Lognormal
Sep	Weibull	Lognormal	SEV	Lognormal	LEV	Weibull
Oct	Exponential	LEV	SEV	LEV	LEV	Weibull
Nov	Zero-Inflated Lognormal	LEV	SEV	Lognormal	LEV	Zero-Inflated Lognormal
Dec	Log Generalized Gamma	Log Generalized Gamma	Weibull	Weibull	Normal	Zero-Inflated Lognormal

can be relied upon as a standard method. The SA main disadvantage is that it is more complicated and need more time to compute as compared to most indices. For SA standardized parameters, drought severity depends on how low S.A is, with an index of below −1 being referred as drought (Jaranilla-Sanchez et al., 2011). A combination of all of the parameters was performed by overlaying the SA indices to determine the extent of severity of droughts in the basin. Temporal variation identified the years and months that were severely affected by droughts as spatial variation identified areas that were drought hotspots in identified months.

3. Study area and dataset

3.1. Study area

The Lhasa River basin is located in the southern part of the Tibetan Plateau in Central Asia. The watershed of the Lhasa River, locally known as Kyi Chu, is the largest and longest river tributary of the upper Brahmaputra River (555 km) that originates from the southern foothills of the Nyaiqentanglha Mountains with a drainage area of 26,225 km^2. The basin has an average annual precipitation of 466.3 mm and monthly average temperature ranges between −9 °C and 9 °C. The geographical coverage of the basin stretches from 29°20′ to 31°15′N and from 90°05′ to 93°20′E as shown in Fig. 3(a). The Lhasa river basin supports agricultural irrigation, township water supplies, and formation of certain traditions of local Tibetans (Lin et al., 2008). The area has glaciers which cover about 600 km^2, which is equivalent to 4 percent of the total basin area. This primary class includes glaciers adhering to mountainsides, and consists of the cirque, niche and crater glacier types as well as hanging glaciers and groups of small ice units (Prasch, 2010).

The basin elevation ranges from approximately 3624–6543 m above mean sea level and land use is dominated by grassland. It is composed of various vegetation types, including alpine steppe, alpine shrub steppe, alpine meadow, and cushion vegetation. The soil type in the area includes alpine meadow soils, shrub-steppe soils, and sub-alpine meadow soils, which are characterized by a clear vertical spectrum. The area also experiences seasonally frozen ground whose length of time has a large impact on agricultural production. In addition to frozen ground, glaciers develop around the drainage basin and headwater region, which also contributes significantly to total runoff primarily during the summer (Lin et al., 2008).

3.2. DEM, land-use and soil data

For accurate simulation and validation of climatic conditions, highly accurate data is required. Therefore, the Lhasa River Basin required a high-resolution data to accurately represent conditions

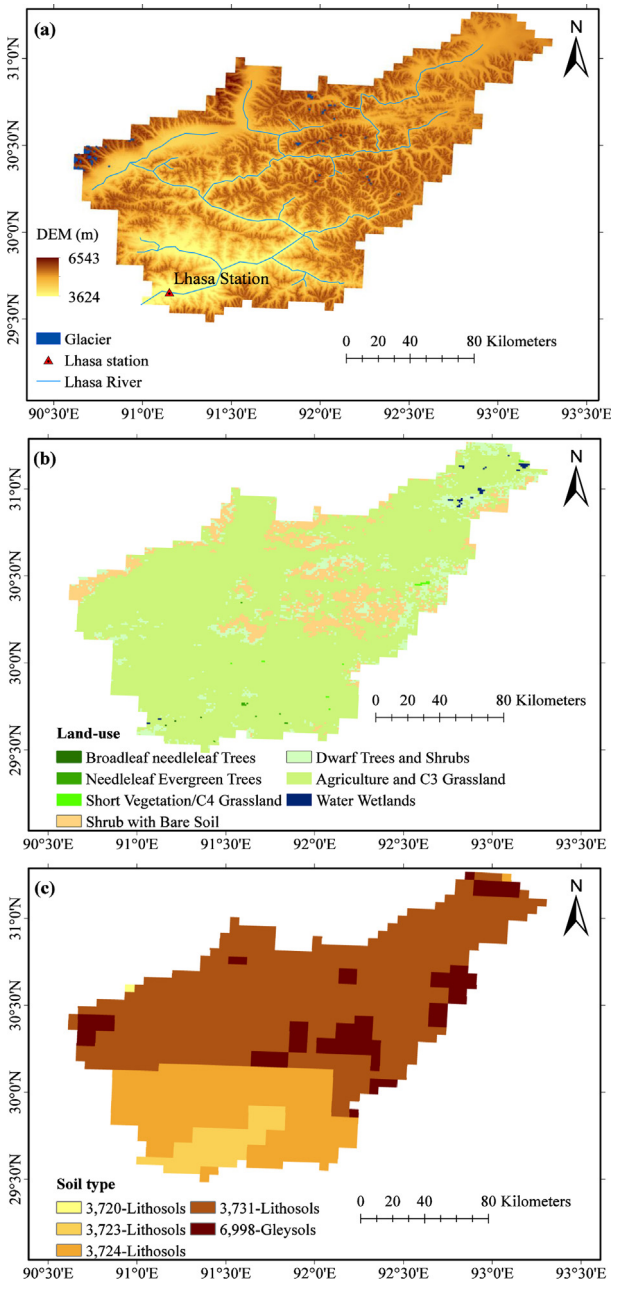

Fig. 3. The Lhasa River basin: (a) digital elevation model, (b) Land-use and (c) Food and Agriculture Organization of the United Nations (FAO) soil type, with river network and discharge gauge station in Lhasa city.

in the basin, especially due to the variability of rainfall over a small area. To achieve this, high-resolution data were used in this study (see Table 2). The Shuttle Radar Topography Mission (SRTM) 90 m Digital Elevation Model (DEM) shown in Fig. 3(a) was obtained from the Consultative Group for International Agricultural Research (CGRIAR) consortium for spatial elevation information. Due to the size of the basin, a reasonable 5-km grid size spatial resolution was used in the study. The DEM was used in basin delineation, subdivision and also in the determination of basin hillslope. Land use data (see Fig. 3(b)) were acquired from the United States Geological Survey. Fig. 3(c) shows soil type classifications according to Food and Agriculture Organization of the United Nations (FAO) obtained from the FAO soils portal. Sellers et al. (1996), defined vegetation parameters composed of morphological, optical and physical properties. For each model grid with one combination of land use type and soil type, the land surface submodel is used to calculate turbulent fluxes between the atmosphere and land surface independently (L. Wang et al., 2010b). The 8-day composite dynamic vegetation properties for the period of study, LAI and FPAR, were obtained from Moderate Resolution Imaging Spectroradiometer (MODIS) Terra Satellite at 1-km spatial resolution, provided by the Earth Observation System Data Getaway for the Aeronautics and Space Administration. LAI and FPAR comprise of morphological, optical and physiological parameters were utilized in WEB-DHM-S as described by Sellers et al. (1996).

3.3. Meteorological and discharge data

The surface meteorological datasets from 1983 to 2012 for air temperature, precipitation, pressure, shortwave radiation, longwave radiation and humidity used in this study were developed by Data Assimilation and Modeling Center for Tibetan Multispheres, Institute of Tibetan Plateau Research, Chinese Academy of Sciences at three hourly time steps by merging satellite data and ground observed meteorological data (Yang et al., 2010; Chen et al., 2011) (see Table 2). The data has a spatial resolution of 0.1 degree and considering the basin is mountainous the issue of quality becomes a big concern. The model had a preset 5 km resolution grid cells which are approximately a half of data spatial resolution, therefore, data quality is not significantly compromised. Spatial distribution of this data was determined by using IDW. The institute also provided daily-observed discharge data for the Lhasa hydrological station.

4. Results and discussion

4.1. Model evaluation

The comparison of monthly discharge between the simulated by the model and the observed shows an adequate representation of both peak and base flow with an NS of 0.78 and RE of −6.99%. Validation of this result was done by extending set conditions to the entire period from 1983 to 2012 which agreed fairly well, with an NS of 0.63 and RE of −8.1% as shown in Fig. 4. To discuss the quality of other model outputs, a validation of simulated soil moisture was done from 2003 to 2008. The validation compares the model simulated soil moisture and observed soil moisture data provided by China Meteorological Administration (CMA). CMA data were recorded after every 10 days except for frozen soil period. The soil was converted from mass percentage to volumetric soil moisture and then aggregated to monthly values within 10 cm and 20 cm soil depth. More information about CMA soil moisture data is given by Wang and Zeng (2011b). The validation resulted into an MBE of 0.005 and RMSE of 0.057 for volumetric 10 cm soil moisture and MBE of −0.019 and RMSE of 0.055 for volumetric 20 cm soil moisture as shown in Fig. 5. Soil moisture was simulated by 5 km grid size data (average of soil moisture within 25 km^2) while observed data was measured at a point, introducing uncertainty in validation hence the differences observed in Fig. 5. Similar trends are expected for groundwater level (validation was not done due to unavailability of groundwater level data in the basin) as hydrological processes are physically based processes.

4.2. Distribution pattern evaluation

Table 3 shows Weibull and log-generalized gamma dominated precipitation distribution functions. For discharge, large extreme values (LEV), normal, lognormal and log-generalized gamma were best-fit distribution functions. Normal, Weibull, logistic and small extreme values (SEV) were identified for surface soil moisture. Root-zone soil moisture distribution patterns were represented by LEV, Weibull and lognormal distributions. Normal and LEV were the only distribution patterns used for groundwater level while log generalized gamma, log-logistic Weibull, normal, lognormal and zero-inflated lognormal distributions were the best-fit distribution pattern for RSG. From the results, it is evident that all variables had a more variable distribution pattern with no dominant best-fit distribution function. Thus, restricting all variables to one distribution function would result in less accurate drought identification results. Details of best-fit distribution functions can be found in Meeker and Escobar (1998).

4.3. Temporal variability of parameters

Fig. 6 shows monthly SA variation, as well as 3-month moving averages for seasonal variation and 12-month moving averages for annual variation for all drought parameters. SA values of less than −1 were observed in most parameters in the years of 1984, 1988, 1995, 1997, 2009 and 2010. Groundwater level SA showed persistent drought conditions from 1992 to 1998, which experienced the worst drought conditions in 1997 (A. Wang et al., 2011). The possible reasons for the persistence have been elucidated by Fan et al. (2005) including an increase in human activities, over-exploitation of the groundwater as well as continuous low precipitation caused the downward trend in the groundwater level during this period. Although the period between 1992 and 1994 shows severe droughts in some parameters (for example groundwater level), this period generally is shown to have experienced mild drought conditions (SA between −1 and zero) in most parameters and therefore it is not considered among drought years. Interestingly, in 1983, SA shows drought in precipitation and soil moisture while other parameters observed mild to no drought conditions. This could be attributed to low precipitation which affected the upper layer of soil and had little effect on root-zone soil and groundwater level as this layers are protected from direct evaporation thus retaining water for a longer period, discharge was supplemented by RSG and base flow hence staying drought free. Monthly SA for observed precipitation and simulated RSG exhibited sporadic variation due to high temporal changes in respective amounts. Twelve-month moving averages in both showed little variation, suggesting that there were no meteorological droughts considering precipitation whereas use of RSG shows 2009 and 2010 droughts. The 3-month moving averages depicted drought adequately for all parameters.

Drought occurrence in the listed years varied in severity across different months. Therefore, selected years were evaluated to determine months that were severely affected by the droughts (Fig. 7). In 1984, extreme drought conditions were observed for soil moisture in August, November and December, severe drought for discharge and RSG in August while moderately dry conditions were observed for precipitation and groundwater level in August and

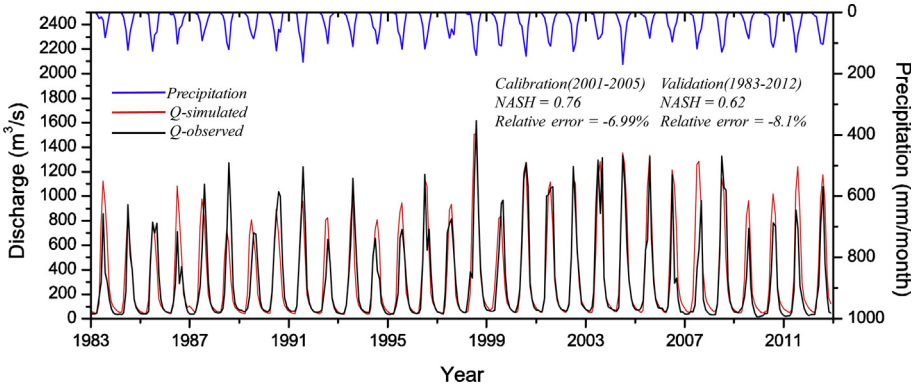

Fig. 4. Simulated (WEB-DHM) and observed monthly discharges in Lhasa River basin during 1983–2012.

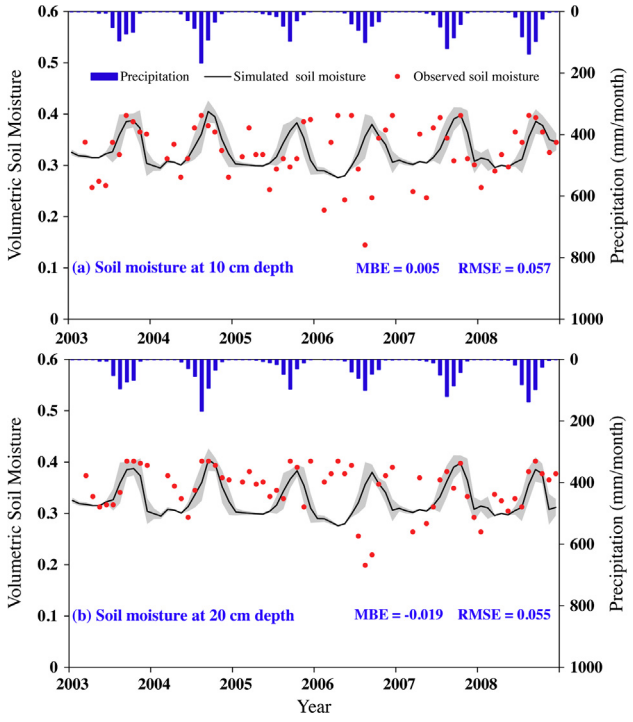

Fig. 5. Validation of simulated (WEB-DHM) soil moisture using observed soil moisture for the station at (29°15′N, 90°46′E) for 2003–2008.

September. From the analysis of all parameters during the year, the month of August was the most severely affected by drought conditions. In 1988, extreme drought conditions were observed for surface soil moisture in the months of July, August and September. Severe drought conditions affected the basin in April, May and July. In addition, similar conditions were observed in September, November and December for root-zone soil moisture while for discharge it occurred in August and September. Moderate drought conditions occurred for precipitation and RSG in September while no drought conditions were observed for groundwater level. In 1995, there were no extreme drought conditions for any of the parameters, but severe droughts were experienced in July for RSG and in January, February March, April and May for groundwater level. Moderate drought conditions occurred in April for both surface soil moisture and precipitation while for discharge it occurred in January, February, March, April and May. Root-zone soil moisture was drought-free except in April and July, which experienced mild drought conditions. In 1997, all parameters experienced moderate drought except for surface soil moisture. Groundwater level experienced droughts in all months with the months of May, June, July and August having severe droughts. In 2009, no drought conditions were observed for groundwater level. Moderate drought conditions occurred in April and August for precipitation, April and June for RSG, April, May and June for discharge, May for surface soil moisture and May, July and October for root-zone soil moisture. In 2010, extreme droughts were observed in June for discharge, precipitation and RSG parameters. Moderate drought occurred in June for surface soil moisture and in May and June for root-zone soil moisture. From the above analysis, months that were severely affected by droughts after consideration of all parameters included August 1984, September 1988, July1995, August 1997, June 2009 and June 2010.

4.4. Spatial drought variability in the Lhasa basin

Like many high altitude mountainous basins, the Lhasa river basin is vulnerable to the impact of global warming due to the presence of glaciers and snow and the sensitivity of the ecosystem enhances the occurrence of extreme weather conditions and natural catastrophes (Akhtar et al., 2008). The impact of these changes varies spatially over the basin (Beniston et al., 1996). There are primary and secondary effects that might result in spatial variations. Primary effects include changes in air density, vapor pressure, increased solar variation receipt, annual/diurnal temperature range, cloud, precipitation distribution as a result of slope and aspect and spatial contrast in solar radiation. Secondary effects included changes in wind velocity, evaporation, snowline altitude, snow proportion and snow cover related to topography.

Spatial analysis was performed for months identified in the temporal analysis of droughts to have experienced the worst net effects of droughts. Hotspot identification was achieved through the spatial representation of SA for all variables involved in droughts quantification as shown in Fig. 8. For droughts involving more than one parameter (agricultural and hydrological droughts), individual parameters' SA were overlaid to determine drought hotspots which are important for identification and monitoring of drought prone areas. Previously, cold region basins such as Lhasa dryness and wetness were based on the precipitation index (SPI) (Bothe et al., 2011; Bothe et al., 2012a, 2012b; Dash et al., 2006; Shunjiu, 2008; Yan et al., 2010; Yu et al., 2014; Yuan et al., 2010; Zhu et al., 2011). During the winter and early part of the spring, precipitation received is in solid form and this water is not available for use until it melts later in late spring and in summer (Immerzeel et al., 2009; Xu et al., 2009). In addition to snowmelt, glacier melt contributes significantly to basin wetness during the summer.

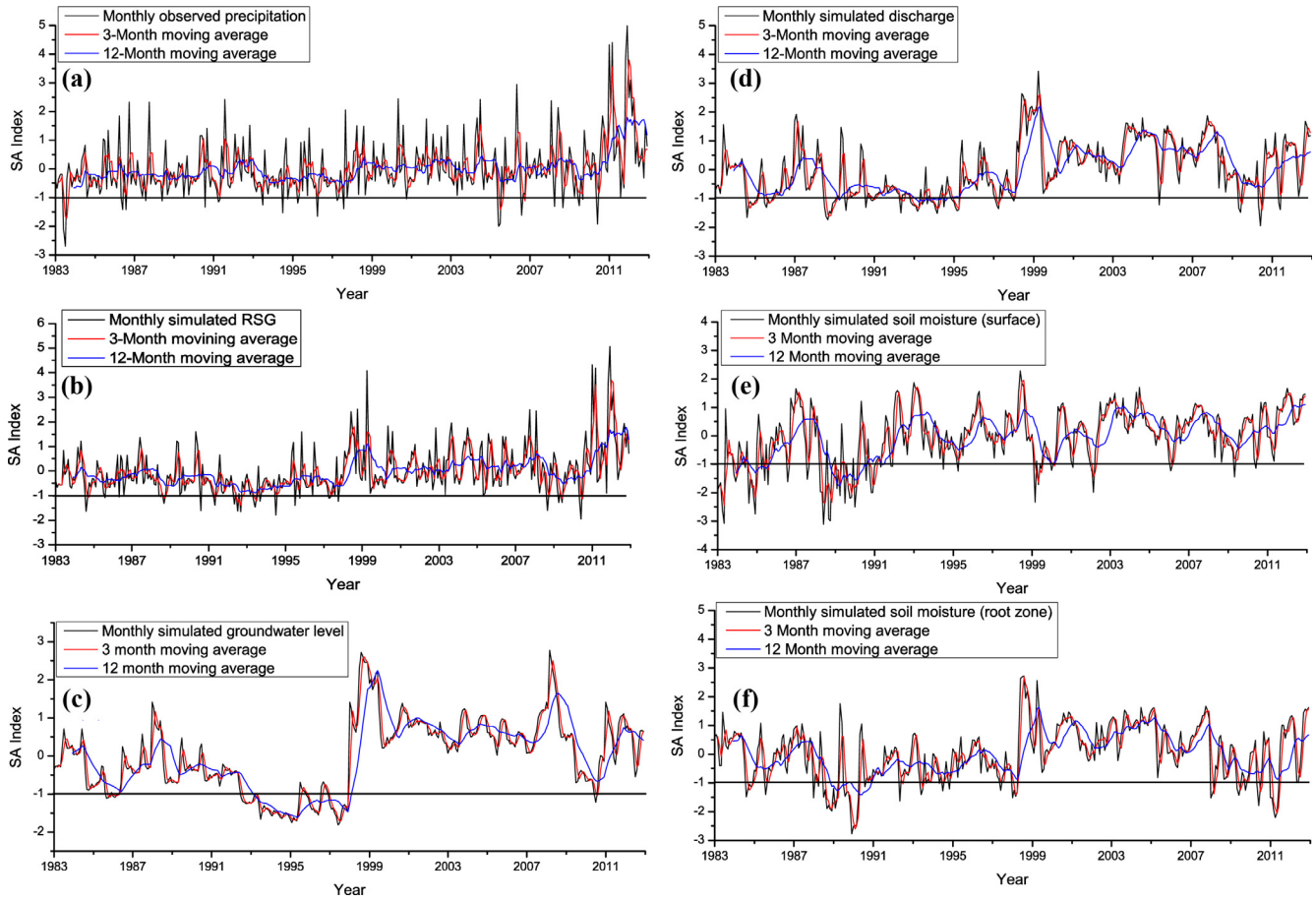

Fig. 6. Standardized anomaly index for monthly, 3-month and 12-month running averaged observed precipitation (a), and simulated RSG (b), groundwater level (c), discharge (d), soil moisture at surface and root zone (e and f) for 1983–2012 for the Lhasa river basin. (Drought occurrence: 1984, 1988, 1995, 1997, 2009 and 2010.)

Precipitation SA distribution patterns seem different from other variables especially in 1988, 1995 and 2009. In 1984, the lower reach of the basin experienced severe droughts in almost all variables, drought conditions were severe in precipitation and soil moisture (agricultural drought). The middle reach of the basin experienced extreme drought conditions in soil moisture, severe drought conditions in groundwater level and discharge (hydrological drought) as well as moderate conditions in precipitation and RSG. The upper reach of the basin experienced mild to moderate conditions in all parameters. In 1988, the middle reach of the basin experienced severe drought conditions in soil moisture, groundwater level and discharge while moderate conditions were observed for RSG. The basin's upper reach observed moderate to severe drought conditions whereas other parameters were largely drought free. In 1995, the basin experienced the least drought condition compared to other drought years. Most areas of the basin were drought free, few areas experienced moderate to severe conditions in soil moisture. Precipitation SA patterns were not consistent with other parameters; this could be mainly due to the significance of RSG contribution to drought on the basin as RSG SA patterns are identical to those of other parameters. 1997 is an interesting year as the basin observed similar drought patterns in precipitation and RSG. The most likely reason for this could be a combination of low precipitation which resulted into severe droughts in precipitation and low temperatures which when coupled with reduced snowfall (as a result of low precipitation) results into reduced RSG thus leading to RSG drought. Discharge and groundwater level drought conditions were spread all over the basin whereas soil moisture drought affected the lower reach of Lhasa River basin. The year 2009 and 2010 experienced similar drought conditions as the middle reach of the basin was drought free. Soil moisture drought was more severe compared to other parameters. All parameters were combined by overlaying (summing SA based on spatial location) (Jaranilla-Sanchez et al., 2011) all the indicators without weighing to highlight drought hotspots. From the overlay, 1984 and 1997 were most drought affected years in Lhasa River basin as no particular area was drought free from analysis of all parameters. Finally, from the spatial distribution of all parameters' SA indices, the similarity in distribution of RSG SA and hydrological drought (combined discharge and groundwater level SA) points to RSG being a crucial indicator of basin dryness in cold regions as opposed to precipitation.

4.5. RSG preference over precipitation

Droughts in cold basins have historically been based on precipitation received. This may be true for other regions that are snow- and glacier-free, but may not be true for cold basins in which snow and glacier melts are important regulators of seasonal discharge. Fig. 9 clearly shows that a long-term average (over 30 years) of RSG agreed well with received discharge in the basin. Recorded precipitation was substantially lower than discharge, implying that the extra volume of water contributing to total discharge must have been as a result of an additional source. The monthly mean peak of discharge was observed in July, which corresponds to the monthly mean peak of RSG as opposed to that of precipitation that was recorded in the month of August which means SPI cannot be relied upon in Long-term monitoring of hydrological drought in

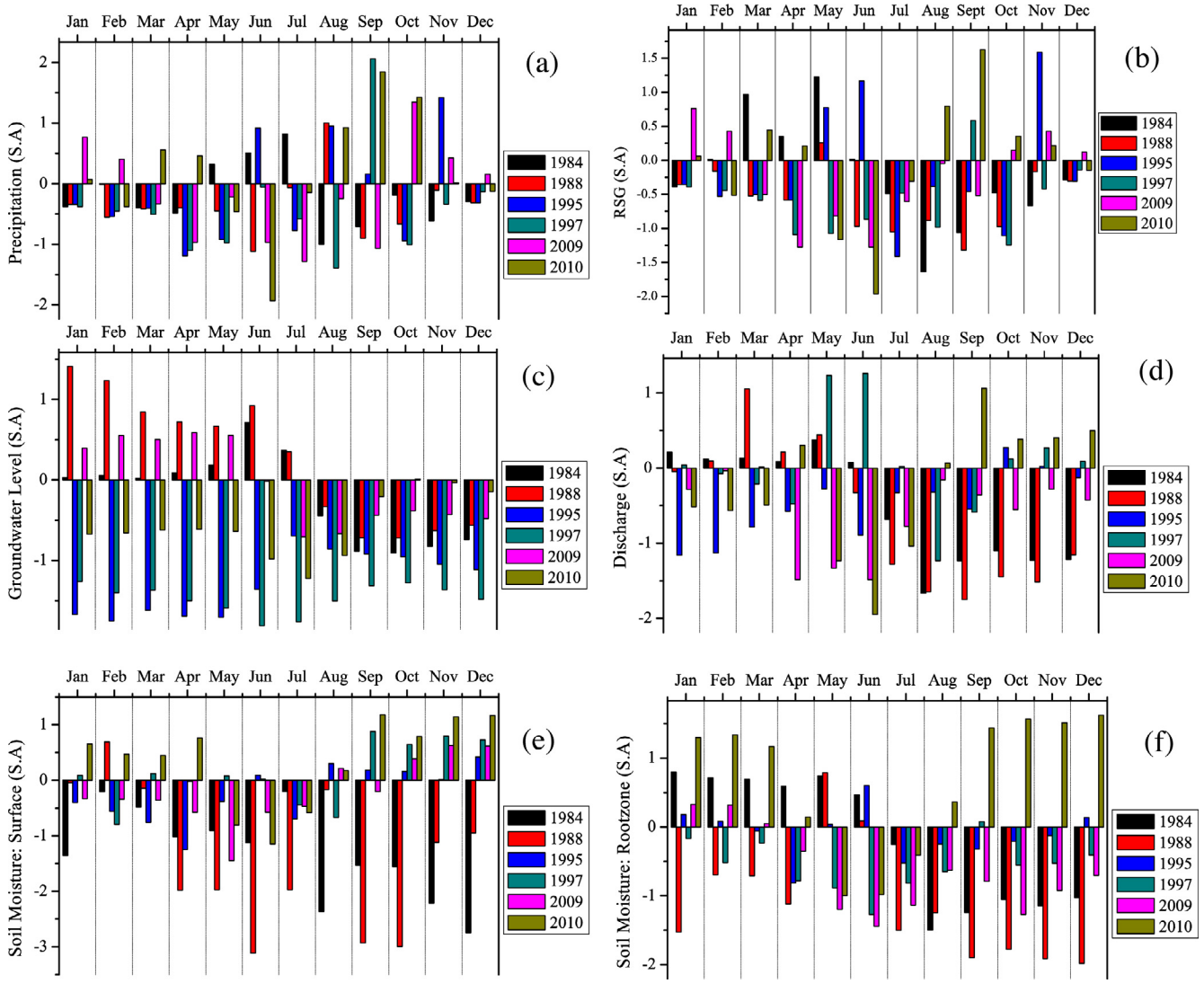

Fig. 7. Standardized anomaly index for the basin average: observed Precipitation (a), and simulated RSG (b), groundwater level (c), discharge (d), soil moisture at surface, and root zone (e and f) for drought years 1984, 1988, 1995, 1997, 2009 and 2010 at Lhasa outlet.

cold basins. The peak month for RSG and discharge was the same as the month with the highest recorded temperatures, which supports the argument that melting of snow and glaciers contributed significantly to total streamflow in the basin. During early spring, the amount of precipitation received was mostly in the form of snow and did not contribute to discharge; hence there was a negative difference between discharge and precipitation (Q-P) as shown in Fig. 10. During early summer, the temperatures were high during the day and dropped significantly during the night and as a result melting occurred during the day to positively contribute to RSG and then water refroze during the night before reaching the streams, thus resulting in negative difference between discharge and RSG (Q-RSG) as shown in Fig. 10. As temperatures continued to increase, the discharge was fed more by snow and glacier melt, hence increasing the peak discharge. During late summer, a positive difference (Q-RSG) was observed, as melted water which was accounted for during early summer melted and fed streams. Spatial differences between RSG and precipitation S.A (RSG-P) shows a big difference in 1984 when drought severely affected the basin, as illustrated in Fig. 11. In August 1984, precipitation overestimated drought conditions in most areas, which experienced extreme droughts in excess of −2.0 (S.A), especially in the lower reaches of the basin. In August 1997 overestimation was slight compared to 1984, with the slight over or underestimation being evenly spread over the whole basin. In June 2009, underestimation of droughts was observed with no area experiencing overestimation. The upper reaches of the basin showed high underestimation in excess of −2.0. The remaining drought years analyzed experienced small difference in most parts, which had minimal effects on the overall meteorological droughts experienced in the basin. The difference shown in Fig. 11 clearly shows the importance of snow and glacier melt consideration in the analysis of droughts in cold regions. The reliability of the precipitation index in the study of drought in such regions is questionable, as it does not show an accurate picture of water availability over the basin.

5. Concluding remarks

This study focused on drought analysis in a typical cold river basin (Lhasa River Basin) from 1983 to 2012. Snow and glacier melt and other variables necessary for drought analysis were modeled using a WEB-DHM-S. Modeled RSG, soil moisture (surface and root-zone), discharge and groundwater level are

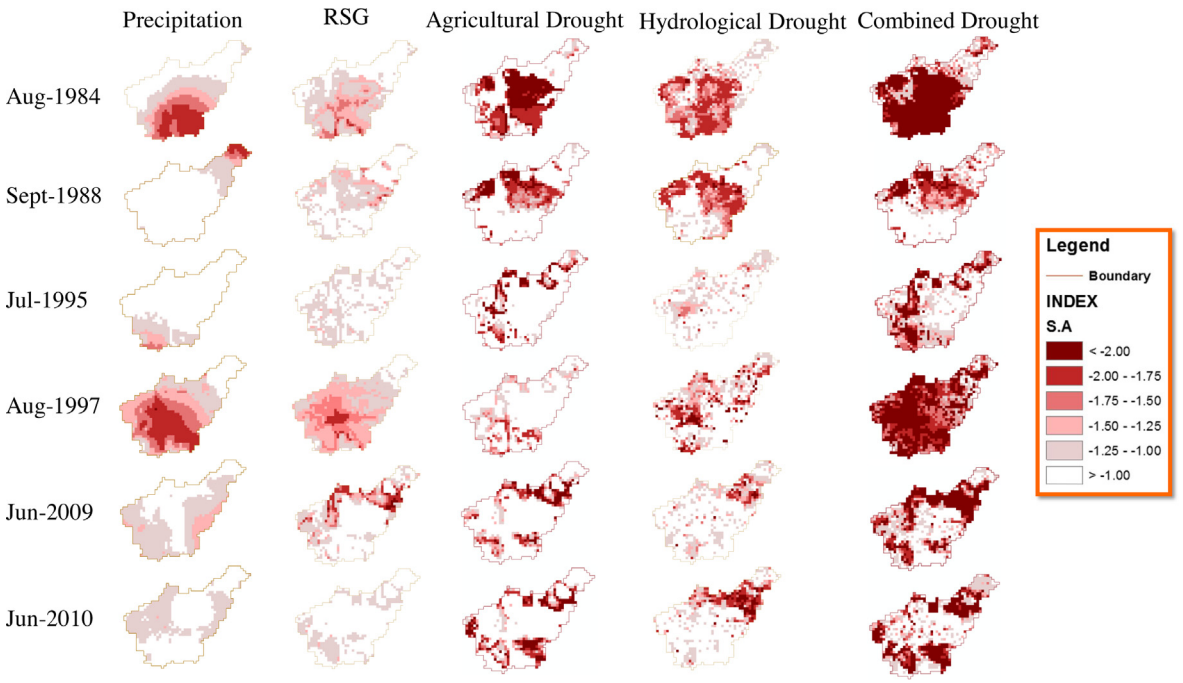

Fig. 8. Spatial representation of the drought severity for August 1984, September 1988, July 1995, August 1997, June 2009 and June 2010 for precipitation drought, agricultural drought (soil moisture), RSG drought, hydrological drought (discharge and groundwater level) and combined drought.

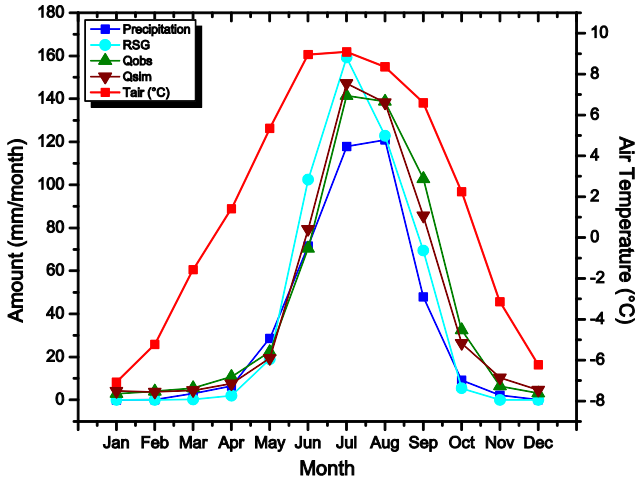

Fig. 9. 30-year monthly averages for observed precipitation (P), simulated rain + snow and glacier (RSG), observed discharge (Qobs), simulated discharge (Qsim), and air temperature (Tair) to illustrate seasonal variability.

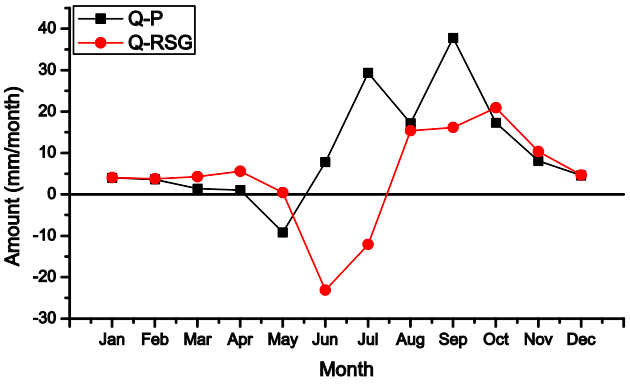

Fig. 10. The difference of discharge and precipitation comparing to the difference between discharge and rain plus snow/glacier melts averaged over 1983–2012.

useful counterparts to climate-based indices, especially in glaciated mountainous cold basins (where getting ground observed data is challenging) for long-term monitoring and sustainable management of drought. Land surface processes govern hydrological conditions in any particular basin thus modeled hydrological variability has a direct relation to climate anomaly as the process is physically based process (all variables have a direct connection). Therefore, model calibration using discharge data was done by adjusting saturated hydraulic conductivity for surface soil, anisotropy ratio which relates hydraulic conductivity in vertical and horizontal planes and maximum surface water storage which account for all water from surface flow, subsurface flow and base flow leading to streamflow, with good calibration results, the model simulated results can be relied upon. In this study, the results from soil moisture validation show consistent results to those of discharge validation.

The study overcame the problem of only using gamma distribution (which has been a major issue in many studies) by considering different distribution patterns to better represent parameters dominated by zeros, extremely low values as well as extremely high values and thus limiting errors resulting from the distribution function. The resultant SA index can be used across all hydrological and meteorological parameters involved in drought analysis as it treats each month for each parameter involved individually by fitting a distribution function and then normalizing to a unique value. With this index, various drought comparison and/or combination based on an overlay of different droughts' SA spatial maps can be achieved, which is different from having different types of indices for different droughts as is the case with many studies. From the analysis, RSG SA distribution pattern agreement with other parameters' SA accept for precipitation reveals RSG can be relied upon to analyze basin dryness as opposed to SPI. Overlaying of all drought indicators revealed moderate to extremely severe drought effects in all drought years (1984, 1988, 1995, 1997, 2009, and 2010). Of all drought years, 1984 and 1997 experienced

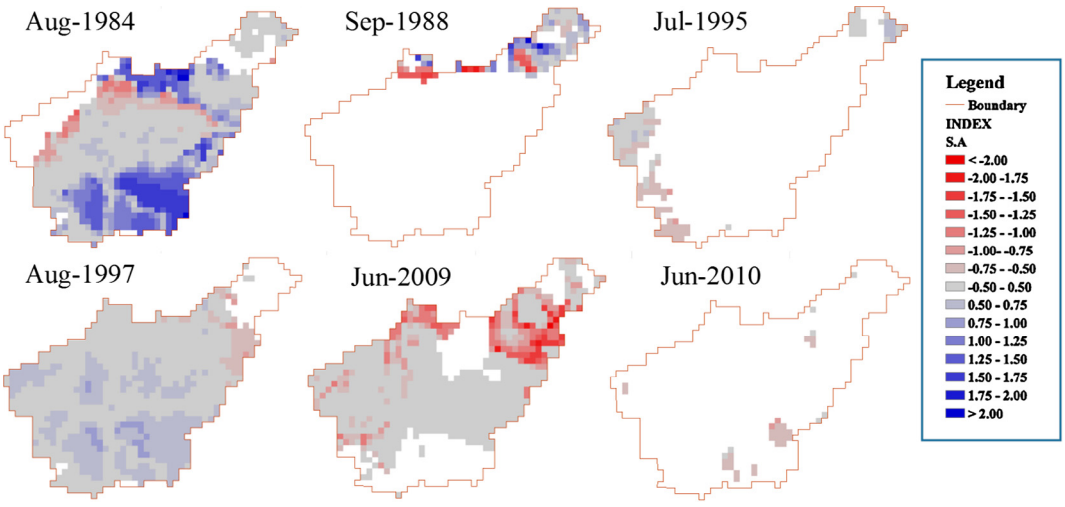

Fig. 11. Spatial analysis showing the difference between RSG SA index and Precipitation SA index for moderately dry to extremely severe drought in August 1984, September 1988, July 1995, August 1997, June 2009 and June 2012.

worse drought conditions with almost all areas experiencing extreme droughts.

Much research has been geared towards improving already-existing indices and there is still much room to further improve the representation of droughts especially in cold regions. In this study, we used a simple glacier model by considering glaciers as thick snow, which can be improved further by considering a more complex physical process-based glacier model to describe relationships between mass balance, ice dynamics and climate to improve simulation of water from the glacier. Based on the fact that drought indices only consider hydrological and meteorological parameters, economic losses as a result of these droughts cannot be quantified by only analyzing indices, as different areas with the same hydrological and meteorological condition will have the same drought conditions even if they have different populations that will directly affect water demand. Therefore, there is a need to also incorporate economic aspects in drought analysis. Different droughts were combined by overlaying individual drought SA maps, the overlaying process was not weighted as there is no formulated way on how to combine various indicators and different parameters are affected by drought differently, which is also subject to prevailing conditions. For this study, overlaying of indicators was solely for drought hotspot identification. More research is needed on how best various droughts can be combined other than just overlaying.

Acknowledgements

This study was financially supported by the National Key Basic Research Program of China (2013CBA01800), the National Natural Science Foundation of China (Grant 41322001, 41190083, and 41571033), the "Strategic Priority Research Program" of the Chinese Academy of Sciences (XDB03030302), CAS-TWAS President's PhD Fellowship Program, the Key Technologies R&D Program of China (2013BAB05B03), and the Top-Notch Young Talents Program of China (Lei Wang). We also wish to thank the editors and four anonymous reviewers for their invaluable comments and constructive suggestions used to improve the quality of the manuscript.

References

Akhtar, M., Ahmad, N., Booij, M., 2008. The impact of climate change on the water resources of Hindukush–Karakorum–Himalaya region under different glacier coverage scenarios. J. Hydrol. 355 (1), 148–163.

Beniston, M. et al., 1996. Impacts of climate change on mountain regions. In: Second Assessment Report of the Intergovernmental Panel on Climate Change (IPCC), pp. 191–213.

Blauhut, V. et al., 2015. Estimating drought risk across Europe from reported drought impacts, hazard indicators and vulnerability factors. Hydrol. Earth Syst. Sci. Discuss. 12, 12515–12566.

Bothe, O., Fraedrich, K., Zhu, X., 2011. Large-scale circulations and Tibetan Plateau summer drought and wetness in a high-resolution climate model. Int. J. Climatol. 31 (6), 832–846.

Bothe, O., Fraedrich, K., Zhu, X., 2012a. Precipitation climate of Central Asia and the large-scale atmospheric circulation. Theoret. Appl. Climatol. 108 (3–4), 345–354.

Bothe, O., Fraedrich, K., Zhu, X., 2012b. Tibetan Plateau summer precipitation: covariability with circulation indices. Theoret. Appl. Climatol. 108 (1–2), 293–300.

Carrão, H., Naumann, G., Barbosa, P., 2016. Mapping global patterns of drought risk: an empirical framework based on sub-national estimates of hazard, exposure and vulnerability. Global Environ. Change 39, 108–124.

Ceglar, A., Zalika, C., Lucka, K., 2008. Analysis of meteorological drought in Slovenia with two drought indices. Proc. BALWOIS, 27–31.

Chanda, K., Maity, R., 2015. Meteorological drought quantification with standardized precipitation anomaly index for the regions with strongly seasonal and periodic precipitation. J. Hydrol. Eng., 06015007

Chen, Y. et al., 2011. Improving land surface temperature modeling for dry land of China. J. Geophys. Res. 116, D20104. http://dx.doi.org/10.1029/2011JD015921.

Dash, S., Shekhar, M., Singh, G., 2006. Simulation of Indian summer monsoon circulation and rainfall using RegCM3. Theoret. Appl. Climatol. 86 (1–4), 161–172.

Dickinson, R.E., Henderson-Sellers, A., Kennedy, P.J., 1993. Biosphere–Atmosphere Transfer Scheme (BATS) Version 1e as coupled to the NCAR Community Climate Model. NCAR Tech. Note NCAR/TN-3871STR, 72p.

Engelhardt, M., Schuler, T., Andreassen, L., 2014. Contribution of snow and glacier melt to discharge for highly glacierised catchments in Norway. Hydrol. Earth Syst. Sci. 18 (2), 511–523.

Esper, J. et al., 2007. Long-term drought severity variations in Morocco. Geophys. Res. Lett. 34 (17), L17702. http://dx.doi.org/10.1029/2007GL030844.

Fan, J. et al., 2005. Dynamic variations and influencing factors of groundwater levels in Lhasa city. Wuhan Univ. J. Nat. Sci. 10 (4), 665–673.

Fendeková, M., Fendek, M., 2012. Groundwater drought in the Nitra river basin-identification and classification. J. Hydrol. Hydromech. 60 (3), 185–193.

Fleig, A.K., Tallaksen, L.M., Hisdal, H., Stahl, K., Hannah, D.M., 2010. Inter-comparison of weather and circulation type classifications for hydrological drought development. Phys. Chem. Earth, Parts A/B/C 35 (9), 507–515.

Gao, J., Williams, M.W., Fu, X., Wang, G., Gong, T., 2012. Spatiotemporal distribution of snow in eastern Tibet and the response to climate change. Remote Sens. Environ. 121, 1–9.

Hao, Z., AghaKouchak, A., 2013. Multivariate standardized drought index: a parametric multi-index model. Adv. Water Resour. 57, 12–18.

Hao, Z., AghaKouchak, A., Nakhjiri, N., Farahmand, A., 2014. Global integrated drought monitoring and prediction system. Sci. data 1. 140001.

Hao, Z., Singh, V.P., 2015. Drought characterization from a multivariate perspective: a review. J. Hydrol. 527, 668–678.

He, Z., Parajka, J., Tian, F., Blöschl, G., 2014. Estimating degree-day factors from MODIS for snowmelt runoff modeling. Hydrol. Earth Syst. Sci. 18 (12), 4773–4789.

Heim Jr, Richard R., 2002. A review of twentieth-century drought indices used in the United States. Bull. Am. Meteorol. Soc. 83 (8), 1149.

Hisdal, H., Tallaksen, L.M., 2003. Estimation of regional meteorological and hydrological drought characteristics: a case study for Denmark. J. Hydrol. 281 (3), 230–247.
Hu, Z., Wang, L., Wang, Z., Hong, Y., Zheng, H., 2015. Quantitative assessment of climate and human impacts on surface water resources in a typical semi-arid watershed in the middle reaches of the Yellow River from 1985 to 2006. Int. J. Climatol. 35 (1), 97–113.
Immerzeel, W.W., Droogers, P., De Jong, S., Bierkens, M., 2009. Large-scale monitoring of snow cover and runoff simulation in Himalayan river basins using remote sensing. Remote Sens. Environ. 113 (1), 40–49.
Jaranilla-Sanchez, P.A., Wang, L., Koike, T., 2010. ENSO influence on the 1982–2000 hydrological properties of the Pantabangan-Carranglan Watershed. Ann. J. Hydraulic Eng. JSCE 54.
Jaranilla-Sanchez, P.A., Wang, L., Koike, T., 2011. Modeling the hydrologic responses of the Pampanga River basin, Philippines: a quantitative approach for identifying droughts. Water Resour. Res. 47 (3).
Klein, A.G., Barnett, A.C., 2003. Validation of daily MODIS snow cover maps of the Upper Rio Grande River Basin for the 2000–2001 snow year. Remote Sens. Environ. 86 (2), 162–176.
Laaha, G. et al., 2016. The European 2015 drought from a hydrological perspective. In: EGU General Assembly Conference Abstracts, p. 16794.
Li, X. et al., 2008. Cryospheric change in China. Global Planet. Change 62 (3), 210–218.
Lin, X. et al., 2008. The trend on runoff variations in the Lhasa River Basin. J. Geog. Sci. 18 (1), 95–106.
Maia, R., Vivas, E., Serralheiro, R., de Carvalho, M., 2015. Socioeconomic evaluation of drought effects. Main principles and application to Guadiana and Algarve case studies. Water Resour. Manage 29 (2), 575–588.
McKee, T.B., Doesken, N.J., Kleist, J., 1993. The relationship of drought frequency and duration to time scales. In: Proceedings of the 8th Conference on Applied Climatology. American Meteorological Society Boston, MA, pp. 179–183.
Meeker, W., Escobar, L., 1998. Statistical Methods for Reliability Data. Wiley, New York.
Meresa, H.K., Osuch, M., Romanowicz, R., 2016. Hydro-meteorological drought projections into the 21-st century for selected Polish catchments. Water 8 (5), 206.
Meyboom, P., 1961. Estimating ground-water recharge from stream hydrographs. J. Geophys. Res. 66 (4), 1203–1214.
Mishra, A.K., Singh, V.P., 2010. A review of drought concepts. J. Hydrol. 391 (1), 202–216.
Nalbantis, I., Tsakiris, G., 2009. Assessment of hydrological drought revisited. Water Resour. Manage 23 (5), 881–897.
Nam, W.-H., Hayes, M.J., Svoboda, M.D., Tadesse, T., Wilhite, D.A., 2015. Drought hazard assessment in the context of climate change for South Korea. Agric. Water Manage. 160, 106–117.
Nash, J., Sutcliffe, J.V., 1970. River flow forecasting through conceptual models Part I—a discussion of principles. J. Hydrol. 10 (3), 282–290.
Ortega-Gaucin, D., Pérez, M.L., Cortés, F.A., 2016. Drought risk management in Mexico: progress and challenges. Int. J. Saf. Secur. Eng. 6 (2), 161–170.
Parajka, J., Blöschl, G., 2008. The value of MODIS snow cover data in validating and calibrating conceptual hydrologic models. J. Hydrol. 358 (3), 240–258.
Posada, D., Buckley, T.R., 2004. Model selection and model averaging in phylogenetics: advantages of Akaike information criterion and Bayesian approaches over likelihood ratio tests. Syst. Biol. 53 (5), 793–808.
Prasch, M., 2010. Distributed Process Oriented Modelling of the Future Impact of Glacier Melt Water on Runoff in the Lhasa River Basin in Tibet. Ludwig-Maximilians-University Munich.
Seçkin, N., Topçu, E., 2016. Drought analysis of the Seyhan Basin by using Standardized Precipitation Index (SPI) and L-moments. Tarım Bilimleri Dergisi 22 (2), 196–215.
Sellers, P.J. et al., 1996. A revised land surface parameterization (SiB2) for atmospheric GCMs. Part II: the generation of global fields of terrestrial biophysical parameters from satellite data. J. Clim. 9 (4), 706–737.
Shrestha, M. et al., 2015. Integrated simulation of snow and glacier melt in water and energy balance-based, distributed hydrological modeling framework at Hunza River Basin of Pakistan Karakoram region. J. Geophys. Res.: Atmos. 120 (10), 4889–4919.
Shrestha, M. et al., 2014a. Optimizing snowfall correction factor for radar-amedas precipitation using distributed snow model (WEB-DHM-S) and modis snow cover data. J. Jpn. Soc. Civ. Eng. Ser. B1 (Hydraulic Eng.) 70 (4), 223–228. http://dx.doi.org/10.2208/jscejhe.70.I_223.
Shrestha, M. et al., 2014b. Correcting basin-scale snowfall in a mountainous basin using a distributed snowmelt model and remote-sensing data. Hydrol. Earth Syst. Sci. 18 (2), 747–761.
Shrestha, M., Wang, L., Koike, T., Xue, Y., Hirabayashi, Y., 2010. Improving the snow physics of WEB-DHM and its point evaluation at the SnowMIP sites. Hydrol. Earth Syst. Sci. 14 (12), 2577–2594.
Shrestha, M., Wang, L., Koike, T., Xue, Y., Hirabayashi, Y., 2012. Modeling the spatial distribution of snow cover in the Dudhkoshi region of the Nepal Himalayas. J. Hydrometeorol. 13 (1), 204–222.
Shukla, S., Steinemann, A.C., Lettenmaier, D.P., 2011. Drought monitoring for Washington State: indicators and applications. J. Hydrometeorol. 12 (1), 66–83.
Shukla, S., Wood, A.W., 2008. Use of a standardized runoff index for characterizing hydrologic drought. Geophys. Res. Lett. 35 (2). http://dx.doi.org/10.1029/2007GL032487.
Shunjiu, W., 2008. Climate change over the eastern part of Tibetan Plateau and the impact on water resources in the upper reaches of Yangtze River. Plateau Mt. Meteorol. Res. 1. 006.
Staudinger, M., Stahl, K., Seibert, J., 2014. A drought index accounting for snow. Water Resour. Res. 50 (10), 7861–7872.
Stefan, S., Ghioca, M., Rimbu, N., Boroneant, C., 2004. Study of meteorological and hydrological drought in southern Romania from observational data. Int. J. Climatol. 24 (7), 871–881.
Sun, S., Xue, Y., 2001. Implementing a new snow scheme in Simplified Simple Biosphere Model (SSiB). Adv. Atmos. Sci. 18, 335–354.
Tallaksen, L.M., Van Lanen, H.A., 2004. Hydrological Drought: Processes and Estimation Methods for Streamflow and Groundwater, vol. 48. Elsevier.
Tekeli, A.E., Akyürek, Z., Şorman, A.A., Şensoy, A., Şorman, A.Ü., 2005. Using MODIS snow cover maps in modeling snowmelt runoff process in the eastern part of Turkey. Remote Sens. Environ. 97 (2), 216–230.
Tijdeman, E., Bachmair, S., Stahl, K., 2015. Controls on hydrologic drought duration in near-natural streamflow in Europe and the USA. Hydrol. Earth Syst. Sci. Discuss. 12, 12877–12910.
Tsakiris, G. et al., 2007. Drought characterization. In: Drought Management Guidelines Technical Annex, pp. 85–102.
Vicente-Serrano, S.M., López-Moreno, J.I., 2005. Hydrological response to different time scales of climatological drought: an evaluation of the Standardized Precipitation Index in a mountainous Mediterranean basin. Hydrol. Earth Syst. Sci. Discuss. 9 (5), 523–533.
Wang, A., Lettenmaier, D.P., Sheffield, J., 2011. Soil moisture drought in China, 1950–2006. J. Clim. 24 (13), 3257–3271.
Wang, A., Zeng, X., 2011. Sensitivities of terrestrial water cycle simulations to the variations of precipitation and air temperature in China. J. Geophys. Res.: Atmos. 116 (D2).
Wang, F. et al., 2011. Evaluation and application of a fine-resolution global data set in a semiarid mesoscale river basin with a distributed biosphere hydrological model. J. Geophys. Res.: Atmos. 116 (D21).
Wang, F. et al., 2012. Ensemble hydrological prediction-based real-time optimization of a multiobjective reservoir during flood season in a semiarid basin with global numerical weather predictions. Water Resour. Res. 48 (7).
Wang, L., Wang, Z., 2006. A distributed hydrological model-GBHNM and its application in middle-scale catchment. J. Glaciol. Geocryol. 28 (2), 256–261.
Wang, L., Koike, T., Yang, D., Yang, K., 2009a. Improving the hydrology of the Simple Biosphere Model 2 and its evaluation within the framework of a distributed hydrological model. Hydrol. Sci. J. 54 (6), 989–1006.
Wang, L. et al., 2009b. Development of a distributed biosphere hydrological model and its evaluation with the Southern Great Plains Experiments (SGP97 and SGP99). J. Geophys. Res.: Atmos. 114 (D8).
Wang, L., Koike, T., Yang, K., Yeh, P.J.-F., 2009c. Assessment of a distributed biosphere hydrological model against streamflow and MODIS land surface temperature in the upper Tone River Basin. J. Hydrol. 377 (1), 21–34.
Wang, L., Koike, T., Yang, K., Jin, R., Li, H., 2010a. Frozen soil parameterization in a distributed biosphere hydrological model. Hydrol. Earth Syst. Sci. 14 (3), 557–571.
Wang, L. et al., 2010b. Development of an integrated modeling system for improved multi-objective reservoir operation. Front. Archit. Civ. Eng. China 4 (1), 47–55.
Wang, L. et al., 2012. Use of integrated observations to improve 0–36 h flood forecasting: development and application of a coupled atmosphere-hydrology system in the Nanpan River Basin, China. J. Meteorol. Soc. Jpn. 90C, 131–144.
Wilhite, D.A., Glantz, M.H., 1985. Understanding: the drought phenomenon: the role of definitions. Water Int. 10 (3), 111–120.
Xu, J. et al., 2009. The melting Himalayas: cascading effects of climate change on water, biodiversity, and livelihoods. Conserv. Biol. 23 (3), 520–530.
Xue, B.L. et al., 2013. Modeling the land surface water and energy cycles of a mesoscale watershed in the central Tibetan Plateau during summer with a distributed hydrological model. J. Geophys. Res.: Atmos. 118 (16), 8857–8868.
Xue, Y., Sun, S., Kahan, D., Jiao, Y., 2003. The impact of parameterizations in snow physics and interface processes on the simulation of snow cover and runoff at several cold region sites. J. Geophys. Res. 108, 8859. http://dx.doi.org/10.1029/2002JD003174.
Yan, F., Wang, Y., Wu, B., 2010. Spatial and temporal distributions of drought in Hebei Province over the past 50 years. Geographical Res. 3, 005.
Yang, D., Herath, S., Musiake, K., 2001. Spatial resolution sensitivity of catchment geomorphologic properties and the effect on hydrological simulation. Hydrol. Process. 15 (11), 2085–2099.
Yang, K., He, J., Tang, W., Qin, J., Cheng, C.C.K., 2010. On downward shortwave and longwave radiations over high altitude regions: observation and modeling in the Tibetan Plateau. Agric. For. Meteorol. 150 (1), 38–46. http://dx.doi.org/10.1016/j.agrformet.2009.08.004.
Yang, Z.-L., Dickinson, R.E., Robock, A., Vinnikov, K.Y., 1997. Validation of the snow submodel of the biosphere-atmosphere transfer scheme with Russian snow cover and meteorological observational data. J. Clim. 10 (2), 353–373.
Yu, M., Li, Q., Hayes, M.J., Svoboda, M.D., Heim, R.R., 2014. Are droughts becoming more frequent or severe in China based on the standardized precipitation evapotranspiration index: 1951–2010? Int. J. Climatol. 34 (3), 545–558.

Yuan, Y., Li, D., An, D., 2010. Winter aridity division in China based on standardized precipitation index and circulation characteristics. J. Desert Res. 30 (4), 917–925.

Zarafshani, K., Sharafi, L., Azadi, H., Van Passel, S., 2016. Vulnerability assessment models to drought: toward a conceptual framework. Sustainability 8 (6), 588.

Zhou, J. et al., 2015. Exploring the water storage changes in the largest lake (Selin Co) over the Tibetan Plateau during 2003–2012 from a basin-wide hydrological modeling. Water Resour. Res. 51 (10), 8060–8086. http://dx.doi.org/10.1002/2014WR015846.

Zhu, X., Bothe, O., Fraedrich, K., 2011. Summer atmospheric bridging between Europe and East Asia: influences on drought and wetness on the Tibetan Plateau. Quatern. Int. 236 (1), 151–157.